kV-Class Lateral NiO_x/GaN Super-Heterojunction Diode via Ammonia Molecular Beam Epitaxy (NH_3-MBE)

Yizheng Liu[1,a)], Zachary J. Biegler[1], Ashley E. Wissel-Garcia[1], James S. Speck[1,a)], and Sriram Krishnamoorthy[1,a)]

[1]*Materials Department, University of California Santa Barbara, Santa Barbara CA 93106, USA*

a) Author(s) to whom correspondence should be addressed. Electronic mail: yizhengliu@ucsb.edu, speck@ucsb.edu, sriramkrishnamoorthy@ucsb.edu

Abstract: This work reports the demonstration of lateral p-NiO_x/p-GaN/n-GaN-based super-heterojunction (SHJ) diodes using p-GaN with additional sputtered p-type nickel oxide (NiO_x) layers to realize charge-balanced structures. The heterojunction diode capacitance-voltage (C-V) model is applied to extract effective the acceptor concentration from the p-NiO_x. Net donor and acceptor concentration in n-GaN and p-GaN are extracted by using metal-oxide-semiconductor (MOS) test structures. The fabricated p-NiO_x/p-GaN/n-GaN SHJ diodes with charge-balanced region between anode and cathode exhibit a forward on-state current density of 10-30 mA/mm across an anode-to-cathode distance (L_{AC}) from 16 μm to 80 μm. The SHJ diodes show rectifying behavior with a maximum on/off ratio of 10^9 and a low reverse leakage density. The highest breakdown voltage achieved for the SHJ diodes is ~2.8 kV with reverse leakage density of 10^{-4} mA/mm at ~80% of device's catastrophic breakdown voltage. The SHJ diodes across all types of dimensions exhibit significant breakdown voltage improvements (~6× on average) with ultra-low reverse leakage current compared to corresponding reference structures without a charge-balanced extension, clearly demonstrating the superjunction effect for devices fabricated on GaN epitaxial layer with ~10^{17} cm^{-3} electron density.

Gallium nitride (GaN) and silicon carbide (SiC)-based wide-bandgap (WBG) power devices are increasingly adopted in low/medium voltage (600 V-1.7 kV) applications for electric vehicles (EVs), industrial motor drives, and renewable energy power processing. The performance limit of unipolar devices is constrained by the inherent trade-off between differential specific on-resistance ($R_{on,sp}$) and breakdown voltage (V_{br}) of power switches[1,2]. Charge-balanced superjunction devices offer a pathway to surpass this unipolar power figure of merit (PFOM), and break the trade-off between $R_{on,sp}$ and V_{br}, allowing devices to have high forward conduction via highly doped epilayers while maintaining improved breakdown voltage with a flattened electric field profile that is realized through careful charge-balancing between intentionally acceptor and donor doped regions[3–6]. Extensive research in WBG material-based superjunction devices, particularly in GaN, has been undertaken in recent years in forms of AlGaN/GaN single and multi-channel two dimensional electron gas (2DEG) charge-balanced with p-GaN, accomplishing breakdown voltages of ~8.85 kV and even beyond 10 kV[7–11]. In these reported lateral GaN super-heterojunction diodes, all the devices' active region epilayers are grown by metalorganic vapor chemical deposition (MOCVD), and charge balancing of these layers is accomplished as-deposited or via subsequent plasma-etching. The reverse leakage current density for these fabricated devices under large reverse bias varies significantly. In Xiao, *et al*'s AlGaN/GaN multi-channel 2DEG charge-balanced Schottky barrier diode (SBD) with p-GaN reduced surface electric field (RESURF) region, the reverse leakage current density is $>10^{-2}$ mA/mm reverse bias > 2.5 kV[10]. Han, *et al*'s AlGaN/GaN single channel 2DEG super-heterojunction SBDs can accomplish relatively low reverse leakage at 10^{-5}-10^{-3} mA/mm by introducing angled ion implantation to the superjunction devices' sidewall to eliminate the potential leakage pathway[7,9,11].

Recently, sputtered nickel oxide (NiO_x) has been widely used as an alternative p-type material for fabrication of heterojunction-based charge-balanced devices[6,12–15]. The conductivity of p-NiO_x can be tuned during sputtering by controlling the oxygen-to-argon ratio (O_2/Ar)[15–17]. Literature results indicated that excess O_2 during sputter deposition can enhance the conductivity in the NiO_x, which is possibly attributed to Ni vacancy-mediated transport[18,19] in NiO_x. The equivalent acceptor concentration in sputtered NiO_x can be extracted by using the heterojunction diode capacitance-voltage model below the diode's dispersion frequency[6,14,20], enabling this material to form charge-balanced superjunciton structure with various n-type WBG semiconductors[6,12,14,20,21].

This work presents the fabrication of NiO_x/GaN super-heterojunction (SHJ) lateral diodes by incorporating sputtered p-NiO_x in combination with a thin p-GaN layer to accomplish post-growth charge-balance with ammonia molecular beam epitaxy (NH_3-MBE) grown n-GaN. The fabricated SHJ diodes with both p-GaN and p-NiO_x charge-balancing layers exhibit a forward on-state current density of 10-30 mA/mm across an anode-to-cathode distance (L_{AC}) of 16-80 μm, and low reverse leakage current density at 10^{-6}-10^{-4} mA/mm with a high rectifying ratio (J_{on}/J_{off}) up to $\sim10^9$. Breakdown voltages of the SHJ diodes are 0.94-2.8 kV with increasing L_{AC}, showing up to 6× on average breakdown voltage improvement compared to the SHJ reference diode structures without charge-balanced regions, indicating the beneficial effect of charge-balancing.

To accomplish accurate charge-balance, it is essential to characterize the net apparent charge concentrations in the n-GaN and p-GaN layers, as well as in the sputtered p-NiO_x. The n-GaN doping density characterization test structure, as shown in **Fig. 1(a)**, consisted of a NH_3-MBE grown unintentionally doped (UID) buffer layer (~200 nm) directly on top of a Fe-doped semi-insulating GaN-on-sapphire template, and a n-GaN (Si-doped) active region (~300 nm) capped by a ~100 nm of UID GaN. A metal-oxide-semiconductor (MOS) C-V structure was adopted to characterize the net charge density in n-GaN by using atomic layer deposition (ALD) grown silicon oxide (SiO_2~50 nm) underneath a Ni/Au (50/150 nm) metal stack. The contact to n-GaN was realized by an electron-beam evaporated Ti/Al/Ni/Au (30/120/30/50 nm) metal stack that was subsequently annealed at 820 °C in an ambient nitrogen (N_2) environment. The p-GaN doping density MOS-CV characterization test structure, as shown in **Fig. 1(b)**, was also grown on similar GaN template with a ~300 nm buffer region followed by a ~300 nm Mg-doped active region and capped with a 10~20 nm p^{++} GaN contact layer. For characterization of p-GaN net acceptor concentration, Ni/Au (50/150 nm) was used as the metal stack on top of a sputtered SiO_2 (~50 nm), and large area Pd/Au (50/150 nm) stack served as Ohmic contact. Using MOS structures ensures low reverse leakage and reduced conduction loss under reverse bias for reliable C-V measurements.

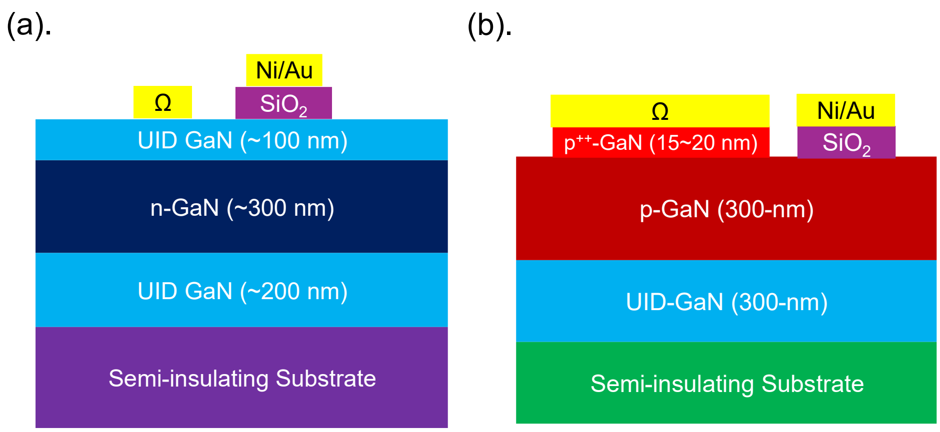

FIG.1. (a) MOS C-V structure of n-GaN SHJ epilayer. (b) MOS C-V structure of p-GaN doping reference epilayer with p^{++} Ohmic contact layer.

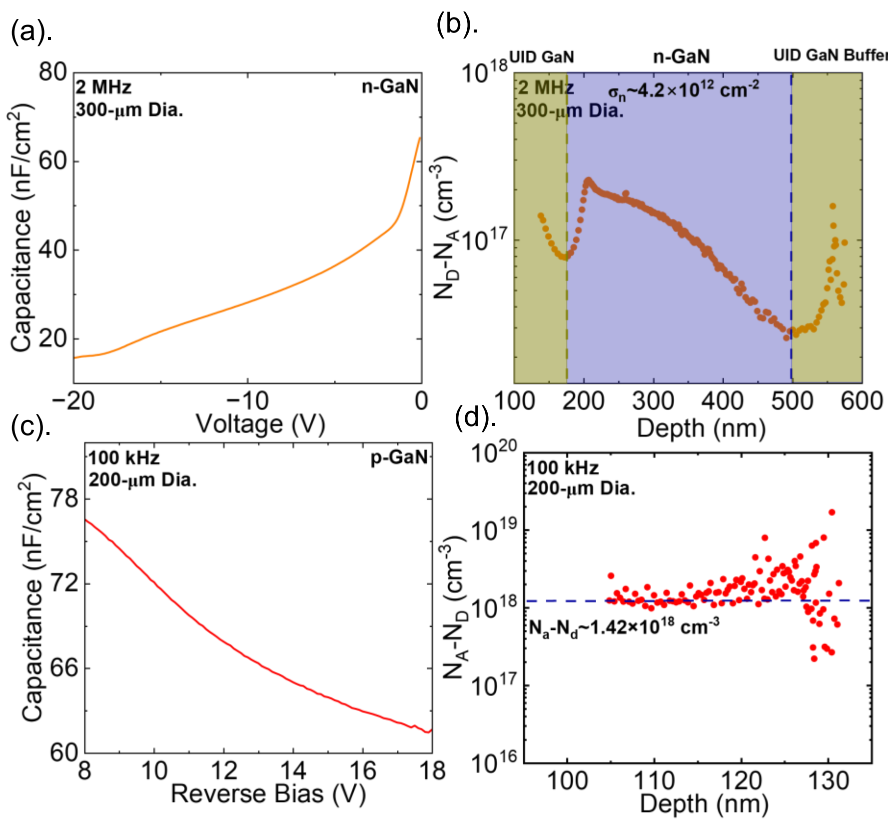

FIG.2. (a) C-V characteristics of MOS n-GaN SHJ epilayer at 2 MHz. (b) Net donor concentration vs. depth profile and a total charge density of 4.2 x 10^{12} cm^{-2} in the n-GaN and

UID-GaN drift region. (c) C-V characteristics of MOS p-GaN SHJ epilayer at 100 kHz. (d) Net acceptor concentration vs. depth profile and a bulk extracted acceptor concentration at 1.42 x 10^{18} cm^{-3}.

The total n-GaN and UID GaN net two-dimensional (2D) sheet ionized impurity density (σ_n) is integrated to be ~4.2×10^{12} cm^{-2} at 2 MHz as shown in **Fig. 2(a) and 2(b)**, closely matching the sheet electron concentration at ~4.9×10^{12} cm^{-2} from room temperature lithographically defined Van Der Pauw Hall effect measurements with an electron mobility of ~501 cm^2/V·s at an bulk net apparent charge density of ~2.5×10^{17} cm^{-3}. The slight reduction of the integrated sheet charge density from C-V measurements is possibly attributed to the incomplete depletion of the UID buffer region near the GaN-on-sapphire template substrate interface, indicating the presence of an interfacial spike carrier density caused by a large concentration of impurities at the regrowth interface[22,23]. Similarly, the p-GaN C-V characteristics at 100 kHz are shown in **Fig. 2(c)** with a net acceptor concentration (N_A-N_D) extracted at 1.42×10^{18} cm^{-3}, as shown in **Fig. 2(d)**

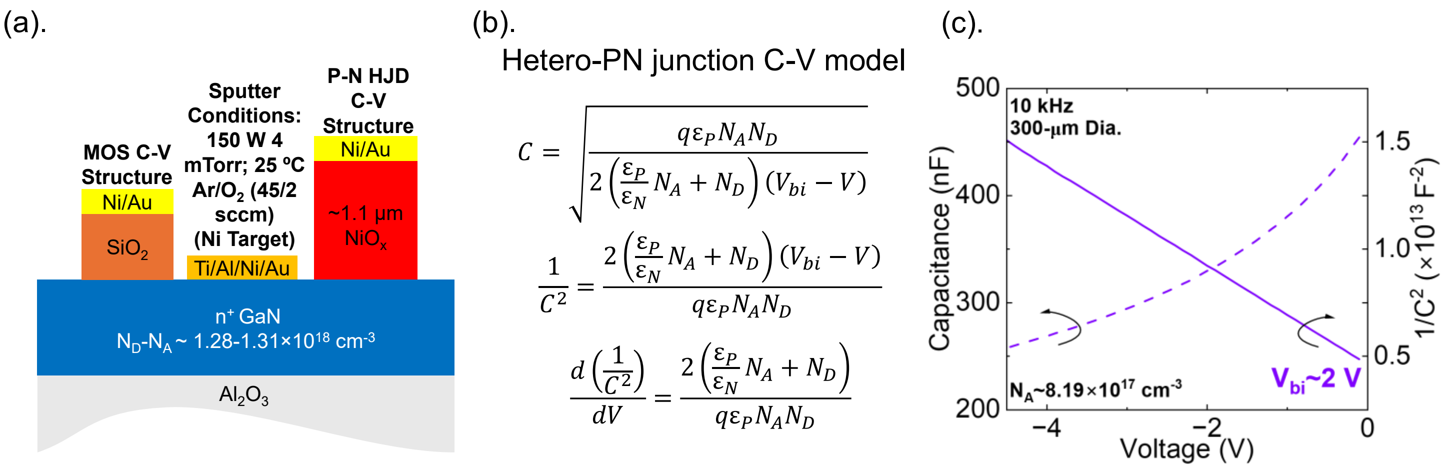

FIG.3. (a) MOS C-V and P-N diode structures for p-NiO_x acceptor concentration (N_A) extraction. (b) Heterojunction P-N diode model for N_a extraction in p-NiO_x. (c) C-V characteristics of p-NiO_x/GaN heterojunction at 10 kHz and $1/C^2$ vs. voltage characteristics.

To extract the acceptor concentration (N_A) in sputtered p-NiO_x, a hetero-PN junction is fabricated on an n^+ GaN-on-sapphire template in **Fig. 3(a)** along with a Schottky MOS C-V structure used for net donor concentration determination in n^+ GaN. Using a highly doped GaN template ensures most of depletion happens in the thick p^- NiO under reverse bias[24], and MOS C-V ensures suitably low conduction loss under reverse bias in the Schottky-based junction for reliable doping concentration (1.28~1.31×10^{18} cm^{-3}) extraction. The p-NiO_x is sputtered via pure metallic Ni target with 45/2 sccm (Ar/O_2) with an RF power of 150 W and chamber pressure of 4 mTorr at room temperature[16,17]. By fitting the hetero-PN junction model in **Fig. 3(b)** using the C-V characteristics in **Fig. 3(c)** at 10 kHz[24], the N_A in sputtered NiO_x is extracted to be ~8.19×10^{17} cm^{-3} with relative permittivity $\varepsilon_{r(NiO)} = 11.9$[24] for NiO_x and $\varepsilon_{r(GaN)} = 8.9$ for GaN[1].

The epitaxial structure of the super-heterojunction (SHJ) diode is shown in the dashed box region in **Fig. 4(a)**. After the superjunction GaN epilayer growth using the same condition as the charge-balance for test structures (**Fig. 1(a) and 1(b)**), the device was fabricated starting with the mesa-isolation of the epitaxial GaN region by reactive ion etching (RIE) using a BCl_3/Cl_2 plasma at 100 W down to the Fe-doped semi-insulating substrates interface. Further patterned dry etching was carried out to remove the p-GaN (~20 nm) and UID GaN (~100 nm) to reach n-GaN active region for the Ohmic contact (cathode) formation. Immediately after dry etching, the wafers were rinsed in de-ionized water and were later submerged into a piranha etch solution (H_2SO_4:H_2O_2 = 3:1, Pure Strip) for 60 minutes to remove organic etching residue from chlorinated photoresist. A 3-minute buffered-oxide etch rinse was then performed to remove the potential oxide/hydroxide on sample surfaces from the piranha etch solution. After the oxide removal, the etched wafer was transferred to a heated 25% concentrated tetramethylammonium hydroxide (TMAH) solution at 50 °C for 5 minutes to remove potential sidewall dry etching damage from the BCl_3/Cl_2 plasma[25]. Finally, a 15-minute rapid thermal anneal (RTA) at 275 °C in the nitrogen (N_2) atmosphere was applied to reduce reverse leakage current on dry etch damaged GaN before cathode metallization[21,26]. The Ti/Al/Ni/Au (30/120/30/50 nm) metal stack was deposited on the n-GaN via e-beam evaporation and RTA annealed at 820 ºC in an N_2 ambient for 30 seconds to form the Ohmic cathode of the SHJ diode. To complete the charge-balance with n-type ionized impurities, the p-NiO_x extension region was sputtered on the planar p-GaN surface and device sidewall using identical deposition condition mentioned earlier in **Fig. 3(a) and 3(c)**. The p-type region and cathode separation distance (L_{PC}) was kept at 3 µm. For practical fabrication of the SHJ diode, if a charge imbalance margin is kept below 15%, the required p-NiO_x thickness (t_{NiOx}) range can be estimated to be 21.9~29.6 nm, and 25.2 nm for the theoretically perfect charge-balance condition using the following relation

$$0.85 < \frac{Q_n}{Q_p} < 1.15 \quad (1)$$

$$0.85 < \frac{4.9\times10^{12}cm^{-2} - (1.42\times10^{18}cm^{-3})(20\times10^{-7}cm)}{(8.19\times10^{18}cm^{-3})t_{NiO_x}} < 1.15 \quad (2)$$

The sputtered NiO_x was then annealed in an N_2 ambient at 275 °C for 15 minutes to stabilize its acceptor concentration[21]. After finalizing the p^- NiO_x charge-balance region, a p^{++} NiO_x contact layer was sputtered (150 W/4 mTorr) with Ar/O_2 flows at 8/10 sccm. Then a self-aligned Ni/Au (50/150 nm) anode Ohmic metal stack was deposited by e-beam evaporation on the device's sidewall and 2-µm extension into the planar p-type region from the mesa edge. The higher percentage of O_2 in the Ar/O_2 mixture induces increased conductivity in the p-type NiO_x for contact improvement[24]. After the metal liftoff from heated N-methyl-2-pyrrolidone (NMP) solution, an epoxy-based negative photoresist (SU-8) was applied to passivate the SHJ diode outside the contact region to mitigate potential electric arcing under high reverse bias[27]. To demonstrate the superjunction effect, reference diodes without the charge-balanced extension

(0% charge-balance) were also fabricated along with the SHJ diodes, simultaneously, as shown in **Fig. 4(a) and 4(b)**.

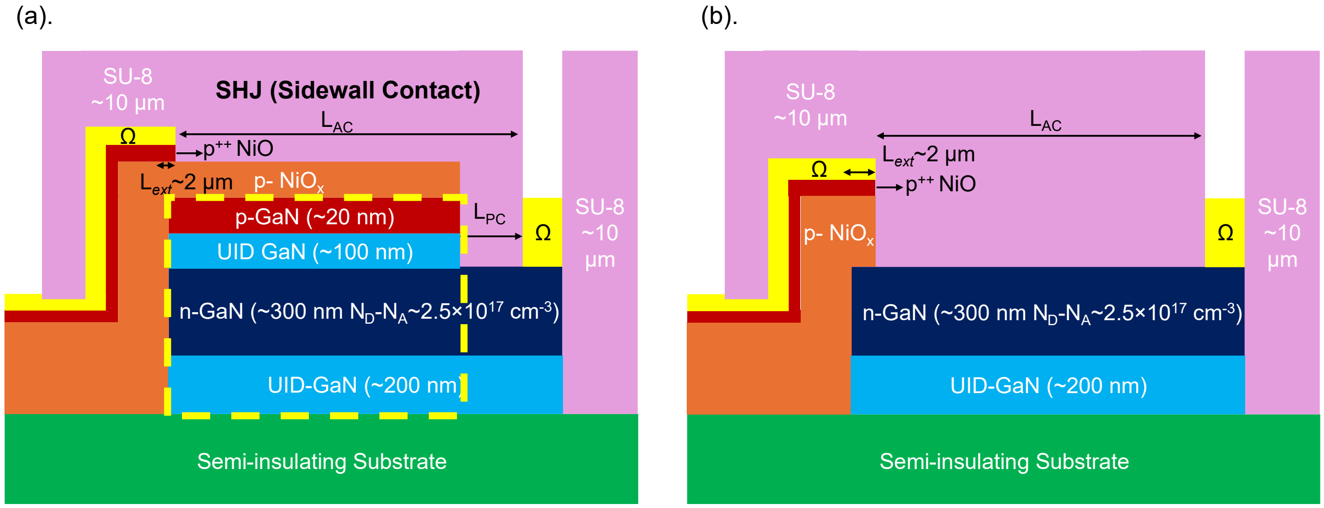

FIG.4. (a) NiO_x/GaN super-heterojunction diode passivated with SU-8. (b) NiO_x/GaN super-heterojunction diode reference structure (0% charge-balance) passivated with SU-8.

Ohmic contacts were obtained for both n-GaN and p-NiO_x characterized by using circular transmission line measurements (CTLMs) test structures with electrode spacings ranging from 5 μm to 15 μm. The extracted sheet resistance from the n-GaN CTLM was at 5 kΩ/□ with a specific contact resistance of 1.21×10^{-7} $\Omega\cdot cm^2$ for annealed Ti/Al/Ni/Au alloyed contact. The p-NiO_x CTLM with a Ni/Au Ohmic stack gives a relatively high sheet resistance of 4.45 GΩ/□.

The super-heterojunction diodes with a 16 μm of anode-to-cathode distance (L_{AC}) exhibited rectifying behavior with an on-state current density reaching ~30 mA/mm at 5 V forward voltage as shown in **Fig. 5(a)**. The reference diode structure without the charge-balanced extension shows similar rectifying behavior but a higher current density at (~40 mA/mm) due to the absence of the vertical depletion region from p-type layers underneath the planar n-GaN top surface[20]. The current density of SHJ diodes decreases as L_{AC} increases, as shown in **Fig. 5(b)-5(d)**. SHJ diodes with all four L_{AC} exhibit rectifying behavior in their semi-log scale J-V characteristics in **Fig. 5(e)-5(h)**, with on-off ratios (J_{on}/J_{off}) of 10^6-10^9 and reverse leakage current densities of 10^{-6}-10^{-4} mA/mm at -5 V on dislocated GaN-on-sapphire template (threading dislocation density ~10^8 cm^{-2}).

The SU-8 passivated SHJ diodes with 16 μm L_{AC} exhibited catastrophic breakdown at 350-940 V with ultra-low reverse leakage current density at ~10^{-5} mA/mm at 80% of devices' breakdown voltage, demonstrating significant breakdown voltage improvements compared to the reference structures, as shown in **Fig. 6(a)**. The breakdown voltages for p-NiO_x/p-GaN/n-GaN SHJ diodes with L_{AC} at 25, 50, and 80 μm were 655-765 V, 1-1.5 kV, and ~2.8 kV, respectively as shown in **Fig. 6(b)-6(d)**, showing substantial device performance improvement compared to their corresponding reference diode structures without charge-balanced extensions. The majority of the SHJ breakdown characteristics showed ultra-low reverse leakage density at 10^{-6}~10^{-4} mA/mm under elevated reverse bias at diodes' 80% breakdown voltages for devices fabricated on highly

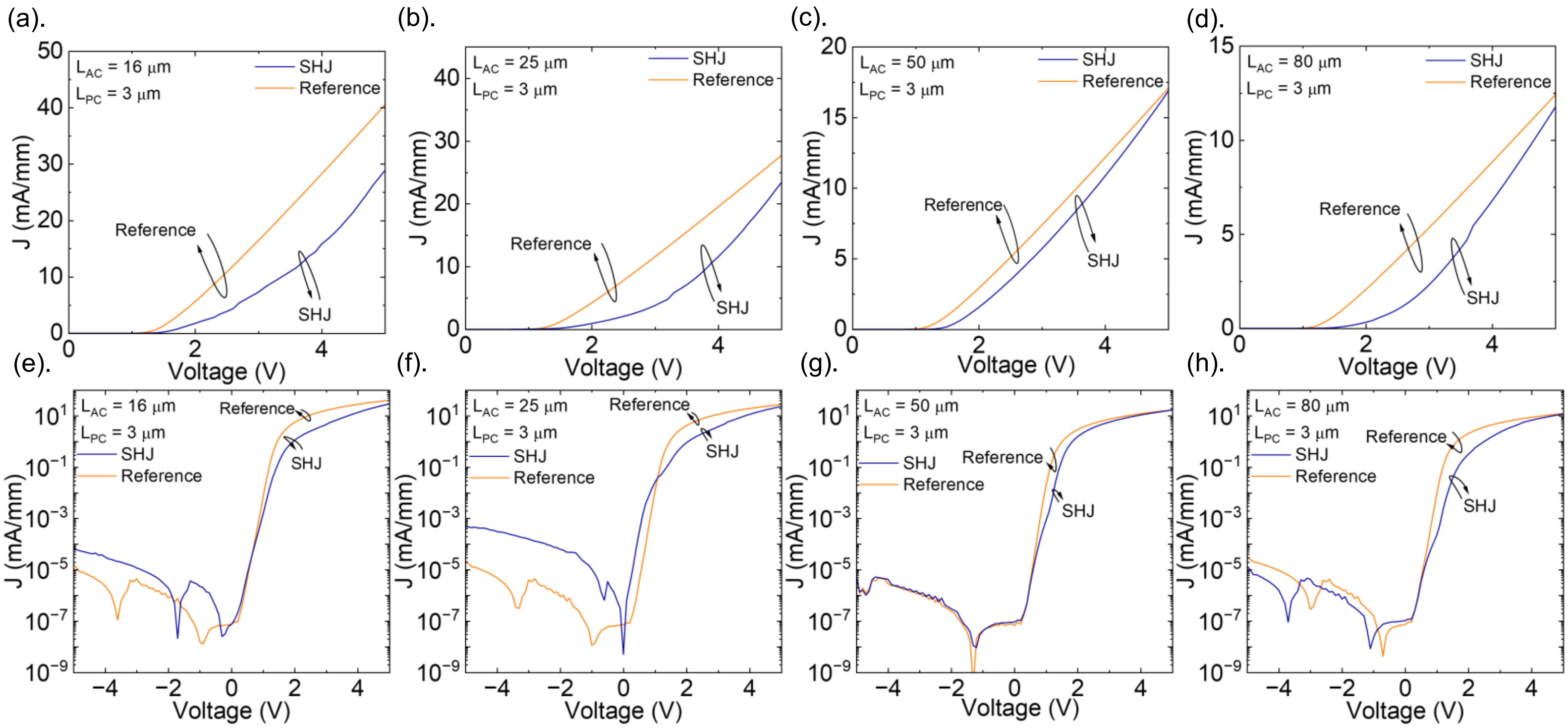

FIG.5. (a)-(d) Linear forward current density vs. voltage characteristics of the NiO_x/GaN SHJ diodes and reference structures with anode-to-cathode distance (L_{AC}) from 16 μm to 80 μm. (e)-(h) Semi-log scale current density vs. voltage characteristics of the NiO_x/GaN SHJ diodes and reference structures with anode-to-cathode distance (L_{AC}) from 16 μm to 80 μm.

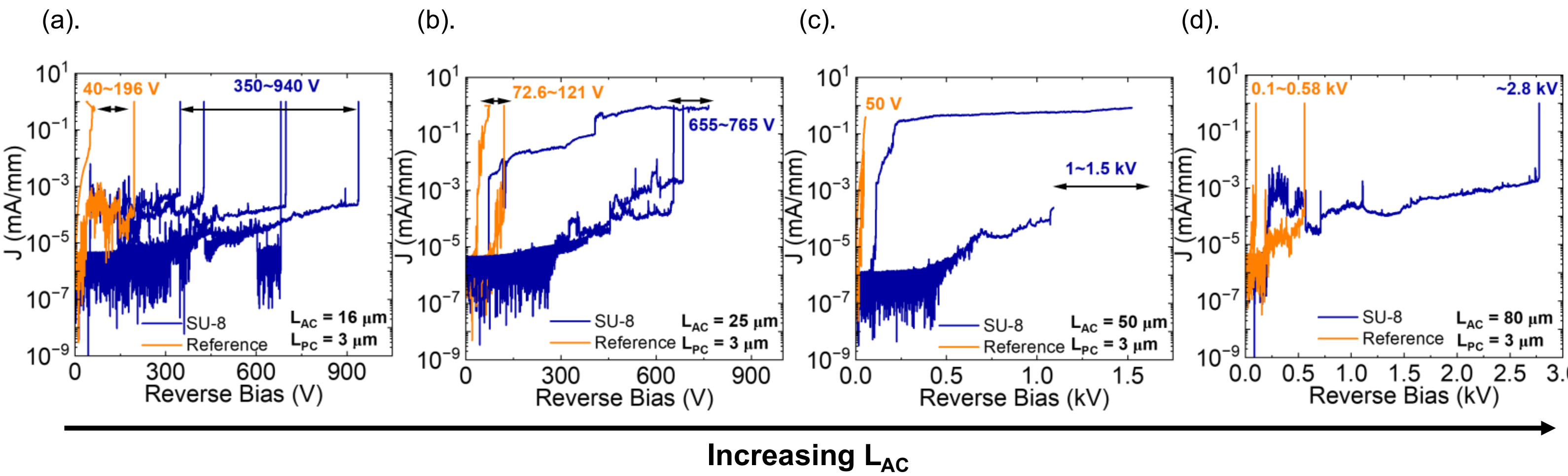

FIG.6. Reverse breakdown characteristics of NiO_x/GaN SHJ diode and reference structures with L_{AC} at (a) 16 μm, (b) 25 μm, (c) 50 μm, and (d) 80 μm.

dislocated GaN-on-sapphire templates, demonstrating comparable performance in terms of reverse leakage current density compared to current state-of-the-art AlGaN/GaN-based superjunction devices[7–10]. The highest breakdown voltage of the SHJ diodes was accomplished at ~2.8 kV on device with anode-to-cathode distance at 80 μm on the n-GaN active region epilayer with > 1×10^{17} cm^{-3} apparent charge density, clearly demonstrating the superjunction effect compared to reference structures without charge-balanced regions for the NiO_x/GaN SHJ diodes in accomplishing high breakdown voltage without compromising the device's forward on-state conduction performance. To withstand an equivalent blocking voltage, it would otherwise require a conventional one-dimensional diode to have ~1×10^{15} cm^{-3} net n-type doping level over 80 μm, which is challenging to accomplish in current GaN epitaxy, and degrades device's on-state resistance.

In summary, this work demonstrates GaN-based super-heterojunction diodes by using NH_3-MBE-grown GaN epitaxial layers and shows the heterogenous integration of p-NiO_x with GaN for achieving charge-balance. In comparison with the reference structure, the highest breakdown voltage of NiO_x/GaN SHJ is at ~2.8 kV, showing up to 6-fold improvement compared to reference structures without charge-balanced regions and clearly demonstrating the superjunction effect for devices with reasonably conductive on-state performance, that are fabricated on >1×10^{17} cm^{-3} apparent doping density GaN epilayer. The reverse leakage current density at 80% of SHJ diode's breakdown voltage is at 10^{-6}-10^{-4} mA/mm, which is among the lowest reverse leakage current density for GaN superjunction diodes[7–10].

ACKNOWLEDGMENTS

The authors acknowledge funding from the U.S. Department of Energy (DOE) ARPA-E OPEN 2021 program (DE-AR0001591). A portion of this work was performed at the UCSB Nanofabrication Facility, an open access laboratory.

DATA AVAILABILITY

The data that supports the findings of this study are available from the corresponding authors upon reasonable request.

REFERENCES

[1] Y. Zhang, and J.S. Speck, “Importance of shallow hydrogenic dopants and material purity of ultra-wide bandgap semiconductors for vertical power electron devices,” Semiconductor Science and Technology **35**(12), 125018 (2020).

[2] B.J. Baliga, “Schottky Rectifiers,” in *Fundamentals of Power Semiconductor Devices*, edited by B.J. Baliga, (Springer International Publishing, Cham, 2019), pp. 171–206.

[3] R. Ghandi, C. Hitchcock, T. Saha, E. Delgado, and S. Kennerley, “5kV SiC Deep-Implanted Superjunction MOSFETs,” IEEE Electron Device Letters, (2025).

[4] R. Ghandi, A. Bolotnikov, S. Kennerly, C. Hitchcock, P. Tang, and T.P. Chow, “4.5 kV SiC charge-balanced MOSFETs with ultra-low on-resistance,” in *2020 32nd International Symposium on Power Semiconductor Devices and ICs (ISPSD)*, (IEEE, 2020), pp. 126–129.

[5] F. Udrea, G. Deboy, and T. Fujihira, “Superjunction power devices, history, development, and future prospects,” IEEE Transactions on Electron Devices **64**(3), 713–727 (2017).

[6] M. Xiao, Y. Ma, Z. Du, Y. Qin, K. Liu, K. Cheng, F. Udrea, A. Xie, E. Beam, and B. Wang, “First demonstration of vertical superjunction diode in GaN,” in *2022 International Electron Devices Meeting (IEDM)*, (IEEE, 2022), pp. 35–6.

[7] S.-W. Han, M. Sadek, J.T. Kemmerling, R. Guan, and R. Chu, “8.85-kV/0.72-A charge-balanced GaN super-heterojunction Schottky barrier diode,” in *2022 6th IEEE Electron Devices Technology & Manufacturing Conference (EDTM)*, (IEEE, 2022), pp. 119–121.

[8] J.T. Kemmerling, R. Guan, M. Sadek, Y. Xiong, J. Song, S.-W. Han, S. Isukapati, W. Sung, and R. Chu, “GaN super-heterojunction FETs with 10-kV blocking and 3-kV dynamic switching,” IEEE Transactions on Electron Devices **71**(2), 1153–1159 (2024).

[9] S.-W. Han, J. Song, M. Sadek, A. Molina, M.A. Ebrish, S.E. Mohney, T.J. Anderson, and R. Chu, “12.5 kV GaN super-heterojunction Schottky barrier diodes,” IEEE Transactions on Electron Devices **68**(11), 5736–5741 (2021).

[10] M. Xiao, Y. Ma, K. Liu, K. Cheng, and Y. Zhang, “10 kv, 39 mΩ· cm^2 multi-channel algan/gan schottky barrier diodes,” IEEE Electron Device Letters **42**(6), 808–811 (2021).

[11] M. Sadek, S.-W. Han, A. Chakravorty, J.T. Kemmerling, R. Guan, J. Song, Y. Xiong, J. Lundh, K.D. Hobart, and T.J. Anderson, “Leakage current and breakdown characteristics of isolation in gallium nitride lateral power devices,” IEEE Transactions on Electron Devices, (2024).

[12] Y. Qin, Z. Yang, H. Gong, A.G. Jacobs, J. Spencer, M. Porter, B. Wang, K. Sasaki, C.-H. Lin, and M. Tadjer, “10 kV, 250° C Operational, Enhancement-Mode Ga_2O_3 JFET with Charge-

Balance and Hybrid-Drain Designs," in *2024 IEEE International Electron Devices Meeting (IEDM)*, (IEEE, 2024), pp. 1–4.

[13] Y. Qin, Y. Ma, M. Xiao, M. Porter, F. Udrea, H. Wang, and Y. Zhang, "(Ultra-) wide-bandgap heterogeneous superjunction: Design, performance limit, and experimental demonstration," IEEE Transactions on Electron Devices, (2024).

[14] Y. Qin, M. Porter, M. Xiao, Z. Du, H. Zhang, Y. Ma, J. Spencer, B. Wang, Q. Song, and K. Sasaki, "2 kV, 0.7 mΩ• cm^2 Vertical Ga_2O_3 Superjunction Schottky Rectifier with Dynamic Robustness," in *2023 International Electron Devices Meeting (IEDM)*, (IEEE, 2023), pp. 1–4.

[15] M.A. Porter, Y. Ma, Y. Qin, and Y. Zhang, "P-Type Doping Control of Magnetron Sputtered NiO for High Voltage UWBG Device Structures," in *2023 IEEE 10th Workshop on Wide Bandgap Power Devices & Applications (WiPDA)*, (IEEE, 2023), pp. 1–7.

[16] Y. Liu, S. Roy, C. Peterson, A. Bhattacharyya, and S. Krishnamoorthy, "Ultra-low reverse leakage NiO_x/β-Ga_2O_3 heterojunction diode achieving breakdown voltage> 3 kV with plasma etch field-termination," AIP Advances **15**(1), (2025).

[17] Y. Liu, S.M. Witsell, J.F. Conley, and S. Krishnamoorthy, "Orientation-dependent β-Ga_2O_3 heterojunction diode with atomic layer deposition (ALD) NiO," Applied Physics Letters **127**(12), (2025).

[18] S. Nandy, U.N. Maiti, C.K. Ghosh, and K.K. Chattopadhyay, "Enhanced p-type conductivity and band gap narrowing in heavily Al doped NiO thin films deposited by RF magnetron sputtering," Journal of Physics: Condensed Matter **21**(11), 115804 (2009).

[19] S. Lany, J. Osorio-Guillén, and A. Zunger, "Origins of the doping asymmetry in oxides: Hole doping in NiO versus electron doping in ZnO," Phys. Rev. B **75**(24), (2007).

[20] Y. Qin, M. Xiao, M. Porter, Y. Ma, J. Spencer, Z. Du, A.G. Jacobs, K. Sasaki, H. Wang, and M. Tadjer, "10-kV Ga_2O_3 charge-balance Schottky rectifier operational at 200° C," IEEE Electron Device Letters **44**(8), 1268–1271 (2023).

[21] Y. Qin, M. Xiao, R. Zhang, Q. Xie, T. Palacios, B. Wang, Y. Ma, I. Kravchenko, D.P. Briggs, and D.K. Hensley, "1 kV GaN-on-Si quasi-vertical Schottky rectifier," IEEE Electron Device Letters **44**(7), 1052–1055 (2023).

[22] A. Bhattacharyya, C. Peterson, T. Itoh, S. Roy, J. Cooke, S. Rebollo, P. Ranga, B. Sensale-Rodriguez, and S. Krishnamoorthy, "Enhancing the electron mobility in Si-doped (010) β-Ga_2O_3 films with low-temperature buffer layers," APL Materials **11**(2), (2023).

[23] Z.J. Biegler, A.A. Allerman, and J.S. Speck, "Removal of Si impurities from GaN regrowth interfaces using XeF2," Applied Physics Letters **127**(7), (2025).

[24] Y. Ma, Y. Qin, M. Porter, J. Spencer, Z. Du, M. Xiao, B. Wang, Y. Wang, A.G. Jacobs, H. Wang, M. Tadjer, and Y. Zhang, "Wide-Bandgap Nickel Oxide with Tunable Acceptor Concentration for Multidimensional Power Devices," Adv Elect Materials **11**(1), 2300662 (2025).

[25] Y. Zhang, M. Sun, H.-Y. Wong, Y. Lin, P. Srivastava, C. Hatem, M. Azize, D. Piedra, L. Yu, and T. Sumitomo, "Origin and control of OFF-state leakage current in GaN-on-Si vertical diodes," IEEE Transactions on Electron Devices **62**(7), 2155–2161 (2015).

[26] Q. Zhou, M.O. Manasreh, M. Pophristic, S. Guo, and I.T. Ferguson, "Observation of nitrogen vacancy in proton-irradiated Al x Ga 1- x N," Applied Physics Letters **79**(18), 2901–2903 (2001).

[27] S. Sharma, K. Zeng, S. Saha, and U. Singisetti, "Field-plated lateral Ga_2O_3 MOSFETs with polymer passivation and 8.03 kV breakdown voltage," IEEE Electron Device Letters **41**(6), 836–839 (2020).